Atmospheric pressure dual RF-LF frequency discharge: Influence of LF voltage amplitude on the RF discharge behavior

Romain Magnan, G J M Hagelaar, Mohamed Chaker, Françoise F. Massines

Plasma Sources Science and Technology

Atmospheric pressure dual RF-LF frequency discharge: Influence of LF voltage amplitude on the RF discharge behavior

To cite this article before publication: Romain Magnan *et al* 2019 *Plasma Sources Sci. Technol.* in press https://doi.org/10.1088/1361-6595/ab4cfe

Atmospheric pressure dual RF-LF frequency discharge: Influence of LF voltage amplitude on the RF discharge behavior

Romain MAGNAN[1,2], Gerjan HAGELAAR[3], Mohamed CHAKER[2] and Françoise MASSINES[1*]

[1]Laboratoire Procédés Matériaux et Energie Solaire, PROMES CNRS, UPR 8521, Rambla de la thermodynamique, 66100 Perpignan, France

[2] Institut National de la Recherche Scientifique, 1650 boulevard Lionel Boulet J3X1S2 Varennes, Canada

[3]Laboratoire plasma et conversion d'énergie, UMR5213, 118 Route de Narbonne, 31077 Toulouse, France

[*]Corresponding author

Abstract

This work is a contribution to a better understanding of dual frequency discharge at atmospheric pressure. Based on experiments and numerical modeling, it is focused on radio frequency (5 MHz) – low frequency (50 kHz) plane/plane dielectric barrier discharge in a Penning mixture (Ar-NH_3). The discharge is in the α-RF mode, biased by a LF voltage having an amplitude ranging from 0 to 1300 V. When the LF amplitude increases, there is a threshold (around 600 V for a 2 mm gap) from which the light intensity (experiment) and the ionization level (modelling) drastically increase. In this work the physics of the RF-LF DBD below and above this threshold is studied. Depending on the respective RF and LF polarity, the net voltage applied to the gas is alternatively enhanced or reduced which induces an increase or a decrease of the ionization level. In all cases the ion drift to the cathode due to the LF voltage results in an ion loss and a production of secondary electrons. For a LF voltage amplitude lower than 600 V, the ions loss to the cathode is higher than the ions creation related to the secondary electrons. The consequence is a decrease of the plasma density. This density oscillates at a frequency equal to 2LF: it is maximum each time the LF voltage amplitude is equal to 0 and minimum when the LF voltage amplitude is maximum. For a LF voltage amplitude higher than 600 V, when the LF and RF polarity are the same, the secondary electrons emission is high enough to counterbalance the ion loss, to enhance the bulk ionization and the discharge becomes a γ-RF. The gas voltage is controlled by the dielectric

charge like a low frequency DBD. Around the gas voltage maximum, on each RF cycle, the discharge is alternatively an α-RF and a γ-RF discharge. When the discharge is in the γ mode, the ions flux at the cathode is increased by a factor 40.

Keywords: dielectric barrier discharge (DBD), atmospheric pressure plasma, dual frequency

1 Introduction

The Dielectric Barrier Discharge (DBD) is an easy and robust solution to generate low temperature discharges. DBDs have many applications including polymer treatment [1], ozone generation [2], air flow control [3], plasma medicine [4]. High quality thin films like water barrier [5][6][7][8][9] or antireflective and passivating film for photovoltaic cells [10][11][12][13] are synthesized using diffuse, streamer-free, linear DBD, easy to scale up for in-line production in conditions similar to corona treatment. One of the key issues for applications is the low power of diffuse DBD which often limits the precursor decomposition and the thin film growth rate. Rising the excitation frequency from kilohertz to megahertz is a solution to sharply increase the DBD power level and thus to reduce the processing time [13][14]. The radio frequency DBD (RF-DBD) generates a high electron density of about $10^{11\text{-}12}/cm^3$, with a high mean power injected in the plasma of 10 W/cm^3. The breakdown voltage of the RF-DBD is one third of that of the low frequency DBD (LF-DBD) [15], which makes the RF-DBD easier to operate. In the α-RF mode, the discharge is sustained by the electrons generated in the gas bulk and the dielectric is not necessary to ensure the discharge stability. However, the highest power values are reached in the γ mode where the discharge is sustained by cathode electron emission. In this case, a DBD configuration is required to achieve a diffuse discharge [16][17]. Another specific feature of RF plasmas is that the ions cannot oscillate in the RF electric field. Using an additional low frequency voltage provides a way of extracting the ions from the bulk and to control their flux to the wall.

Dual frequency (DF) excitation was previously investigated in low pressure plasmas to independently control the plasma generation and the ion flux on the surface i.e. the electron heating and

the ion acceleration across the sheath [18][19][20][21]. At atmospheric pressure, the collision rate is large and the previous investigations were focused on the DF influence on the electron energy distribution function (EEDF), as well as on the control of the electron density and of the ion flux to the wall, and on the ionization mode [22][23][24][25]. Most studies were focused on the use of high frequencies (HF) in MHz range, for both excitation frequencies. However, some works combine kHz and MHz [26][27][28] frequencies. In [29][30], Liu *et al* superimpose a RF voltage to a LF-DBD to modulate the electric field, which improves the uniformity of the discharge and increases the input power.

RF voltage leads to a low electron temperature, ion trapping in the plasma bulk and more power transferred to elastic collisions, which enhances gas heating due to vibrational excitation especially in case of nitrogen [31][32]. The low frequency could influence the ion flux to the wall, increase the secondary electron emission and the electron temperature while the high frequency ensures a large plasma density with a higher ionization rate at the sheath edge. Applying a dual frequency modifies the power dissipation and the electron heating mechanism. In a DF plasma (14 MHz-2 MHz) at atmospheric pressure, increasing the voltage amplitude of the LF component induces the transition from the α mode to the γ mode [22]. Observations show a change in the ionization mechanism from wave riding to cathode secondary emission associated to an increase of the electron temperature.

In this work, the discharge initially operates in the α mode at 5 MHz RF frequency. The discharge physics modifications of the RF-DBD induced by the increase of the LF voltage amplitude are investigated using both experiments and 1D-simulation. This study is carried out in an Ar/NH_3 Penning mixture and focuses on the light emission, the plasma ionization dynamics and the species density within the gas gap. The chosen LF frequency is 50 kHz because previous work [33] carried out in the same discharge configuration we have found that the coupling between RF and LF frequencies is maximum for a LF of 50 kHz.

2 Experimental set up

a) b)

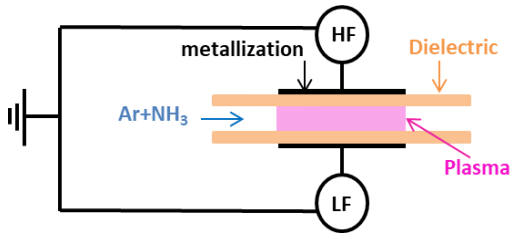

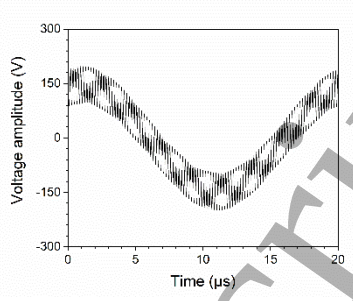

Figure 1. (a) Schematic drawing of the discharge cell and (b) voltage applied between the electrodes f_{HF} = 5 MHz V_{RF} = 350 V and f_{LF} = 50 kHz V_{LF} = 200 V

This section presents the plasma reactor and the characterization methods. The discharge cell is schematically shown in Figure 1 together with the applied voltage. A usual plane to plane dielectric barrier discharge configuration is used inside an airtight chamber. Each electrode has a 1 cm x 5 cm surface and is covered by a dielectric layer (alumina Al_2O_3) of 1 mm thickness. The chamber is pumped and the reactor filled with Argon 2 Alphagaz (Air Liquide) up to the atmospheric pressure. The argon flow rate is 3 l min^{-1} and NH_3 is added with a concentration of 133 ppm in order to obtain a Penning mixture. The gap gas is 2 mm.

The plasma is ignited by applying the RF voltage between one of the electrodes and the ground while the LF voltage is applied between the other electrode and the same ground. Both sinusoidal frequencies are delivered by the same waveform generator (KEYSIGHT 33500B Series) that allows their synchronization. They feed an amplifier connected to a high-voltage transformer. For the RF signal, the waveform generator is connected to a broadband power amplifier (PRANA GN500) operating in the 100 kHz-200 MHz range linked to a homemade transformer that delivers 5 MHz. For the LF signal, the waveform generator is connected to an audio amplifier (Crest CC4000) connected to an up-voltage transformer (Boige & Vignal) designed to operate from 40 to 60 kHz. The electrical measurements are performed using a current probe (LILCO LTD 13W5000) and voltage probes (Tektronic P6015A 75 MHz) connected to an oscilloscope (Tektronix DPO4104 1 GHz). Discharge images are obtained with

an iCCD camera operating in the UV-Visible range (200-900 nm) (PI-MAXII Princeton Instruments) synchronized to the LF or HF applied voltage. The time variation of the emission intensity is measured with a photomultiplier (PMH10721-20 Hamamatsu) centered in the visible range (450-800 nm). In this work, the RF frequency is 5 MHz with a voltage amplitude fixed at 350 V and the LF frequency is 50 kHz with a voltage amplitude varying from 0 to 1300 V.

3 Model description

The discharge is simulated using a 1D self-consistent fluid model, based on a general 2D plasma code previously used for other discharges and described in [34][35], which was adapted to the DBD geometry in 1D Cartesian space. This model solves the electron, ion and metastable continuity and momentum transfer equations coupled to Poisson's equation. The energy equation is also solved for the electrons. The model provides the space and time variations of the electric field and the densities of electrons, Ar^+ and Ar_2^+ ions, and Ar metastables.

3.1 Equations and boundary conditions

The equations for electrons are:

$$\frac{\partial n_e}{\partial t} + \nabla.(\boldsymbol{\Gamma}_e) = S_e \quad (1)$$

$$\boldsymbol{\Gamma}_e = -\mu_e n_e \boldsymbol{E} - D_e \nabla n_e \quad (2)$$

The equations for ions are:

$$\frac{\partial n_i}{\partial t} + \nabla.(\boldsymbol{\Gamma}_i) = S_i \quad (3)$$

$$\boldsymbol{\Gamma}_i = \mu_i n_i \boldsymbol{E} - D_i \nabla n_i \quad (4)$$

where n is the particle density, $\boldsymbol{\Gamma}$ is the particle flux, S is the particle source term due to chemical processes occurring in the plasma, $\boldsymbol{E}$ is the electric field, μ and D are the mobility and the diffusion coefficient, respectively. The equations for the metastable atoms are similar to those for electrons and ions except that their mobility is zero. The electric field is obtained from the electrostatic potential solved from the Poisson equation:

$$\varepsilon_0 \nabla \boldsymbol{E} = -\varepsilon_0 \nabla^2 \phi = -e n_e + \sum_i q_i n_i \quad (5)$$

where ε_0 is the permittivity of free space, ϕ is the electrostatic potential, e is the elementary charge and q_i is the ion particle charge. The summation runs over all ion species.

The equation of energy is solved for electrons:

$$\frac{3}{2}\frac{\partial(n_e k_B T_e)}{\partial t} + \frac{5}{2}\nabla \cdot (\boldsymbol{\Gamma}_e k_B T_e - n_e D_e k_B \nabla T_e) = -e\boldsymbol{\Gamma}_e \cdot \boldsymbol{E} - C \quad (6)$$

where k_B is the Boltzmann constant, T_e is the electron temperature, and C is the density of the net power lost in collisions and plasma-chemical processes. Here, the electron temperature is an effective temperature defined as 2/3 of the electron mean energy, because the electrons are not Maxwellian. This electron temperature is used to obtain the electron mobility, the electron diffusion coefficient and the rate coefficients of all electron-induced processes included in the source terms S and C, from look-up tables obtained from the electron Boltzmann solver BOLSIG+[36] [37].

Boundary conditions are imposed on the particle fluxes at the walls:

$$\boldsymbol{\Gamma}_e \cdot \mathbf{n} = n_e v_{w,e} - \sum_i \gamma_i n_i v_{w,i} \quad (7)$$

$$\boldsymbol{\Gamma}_i \cdot \mathbf{n} = n_i v_{w,i} \quad (8)$$

where **n** is the normal vector pointing toward the wall and v_w is an effective velocity at the wall. These boundary conditions take into account the secondary electrons emission following ion and metastable impact on the walls with a secondary emission coefficient set to 0.05. A similar boundary condition is used for the electron energy flux at the wall. For more information about these boundary conditions we refer the reader to [34].

As a boundary condition for the Poisson's equation, sinusoidal RF and/or LF voltages are imposed at the electrodes. The voltage drop across the dielectrics is self-consistently calculated, taking into account their permittivity and the accumulated surface charge obtained by time-integration of the electron and ion wall fluxes, as in [35]. Each dielectric is 1 mm thick with a relative permittivity of 9.

The list of the considered plasma chemical reactions and their rate coefficients are detailed in Table 1. To simplify the results analysis, Penning ionization of NH_3 is considered without adding NH_3 and NH_3^+, but considering the creation of Ar^+ from Ar metastables using a reaction coefficient corresponding to 200 ppm of NH_3 in Ar. Thus the species considered in the kinetic description are electrons, Ar^+ and Ar_2^+ ions and Ar*. The species Ar* includes all the excited argon states, including the metastable states and the radiative resonant states.

Table 1. Model kinetic reactions and rate coefficients

Reaction		Rate coefficient	Ref
1)	$e + Ar \rightarrow e + Ar^*$	$F(T_e)$	[36][38][39]
2)	$e + Ar_2^+ \rightarrow Ar^* + Ar$	$7.35 \times 10^{-14} \times Te^{-0.67}$ m^3 s^{-1}	[40]
3)	$Ar^* \rightarrow Ar$	1.5×10^6 s^{-1}	
4)	$e + Ar^* \rightarrow e + Ar$	2×10^{-13} m^3 s^{-1}	
5)	$e + Ar^* \rightarrow 2e + Ar^+$	$F(T_e)$	
6)	$e + Ar \rightarrow 2e + Ar^+$	$F(T_e)$	
7)	$2Ar^* \rightarrow Ar + e + Ar^+$	$6{,}4 \times 10^{-16}$ m^3 s^{-1} (branching ration 0.3)	[41]
8)	$2Ar^* \rightarrow e + Ar_2^+$	$6{,}4 \times 10^{-16}$ m^3 s^{-1} (branching ration 0.7)	[41]
9)	$Ar^* \rightarrow e + Ar^+$ (Simulation of NH_3 Penning ionization)	2.06×10^5 s^{-1}	[42]
10)	$Ar^+ + 2Ar \rightarrow Ar_2^+ + Ar$	2.5×10^{-43} m^6 s^{-1}	[42][43]

Reaction 3 represents the radiative losses taking into account all the excited states, the coefficient corresponds to the trapping rate for the radiative reaction. This coefficient was initially taken as 5×10^5 s^{-1} in agreement with [44] but, as discussed in section 3.2, we found that it should be increased up to 1.5×10^6 s^{-1} to achieve a good agreement between numerical and experimental results.

3.2 Validation of the model

To be suitable for the dual frequency DBD, the model should properly describe both RF and LF-DBD. This was verified by comparing numerical and experimental results for a 5 MHz DBD and a 50 kHz DBD obtained at 350 V and 1 kV respectively.

Figure 2 presents the calculated time variations of the current density, the voltage applied to the electrodes, V_a, and the voltage across the gas gap, V_g, for a RF-DBD at 5 MHz-350 V and a LF-DBD at 50 kHz-1000 V.

a) b)

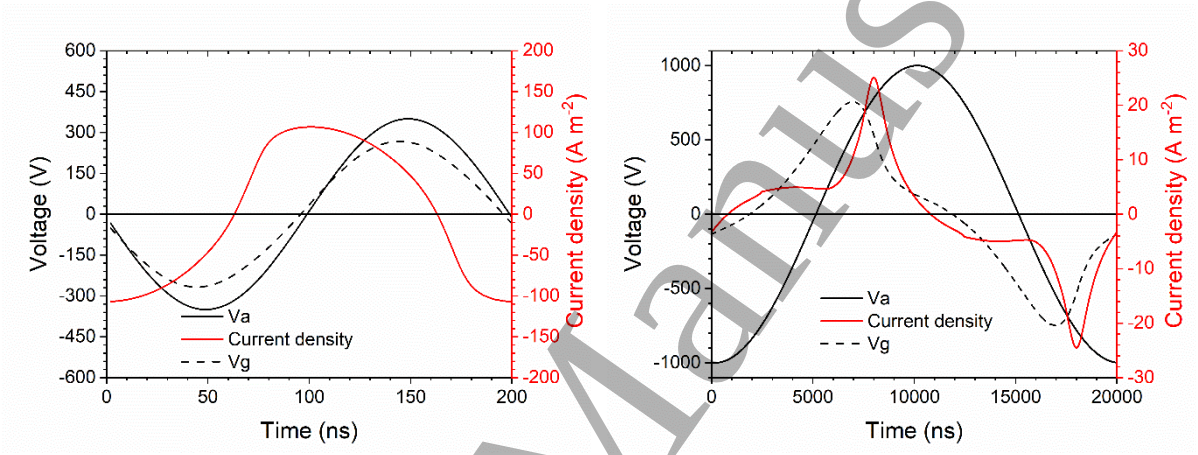

Figure 2. Time-dependence of the voltage applied to the electrodes, V_a, on the voltage across the gas gap, V_g, and on the current density over one cycle for a) RF-DBD (5 MHz, 350 V) and b) LF-DBD (50 kHz, 1 kV) as calculated from the model.

These numerical results are in good agreement with the literature. In RF-DBD (figure 2a), the gas voltage and current are almost sinusoidal. The difference between V_g and V_a is explained by the charging of the dielectric surface, which reflects on the shape of the current density. The phase angle between the current and the voltage is $\pi/2$, corresponding to a typical capacitive discharge at atmospheric pressure [10][45][16][46].

Figure 2b presents the results for the LF-DBD. In agreement with the literature, one current pulse occurs each half cycle. The voltage across the gas gap drastically decreases during the current

pulse. The current pulse is larger than 100 ns and shows a reverse current peak when the voltage polarity changes, both characteristics of a glow DBD [47][48][49][50].

To further confirm the validity of the model, the experimental and numerical density of Ar^3P_2 metastable atoms were compared for RF and LF discharges. The Ar^3P_2 density was measured by laser absorption spectroscopy. In the model, Ar* includes all the excited state of Ar. To calculate the Ar^3P_2 density from the modeling Ar* density, we assume that the four first excited level of Ar are the most occupied. These four excited levels are $^3P_2$, $^1P_1$, $^3P_0$ and $^3P_1$. They are in equilibrium and the distribution on each level is proportional to (2J+1) [51][52][53]. Thus the Ar^3P_2 density is equal to the modeling Ar* density multiplied by 5/(5+3+1+3) =5/12. In the case of the RF discharge, for a frequency of 5 MHz and a voltage amplitude of 350 V, the rate coefficient of reaction 3 (Table 1) was increased in order to reduce both metastable density and power in such a way to obtain similar experimental and numerical results (Table 2). Then, using the same coefficient, experimental and numerical results were compared in the case of the 50 kHz DBD for 1 and 2 mm gap. As presented in Table 2, both experiments and model predictions agree within a factor lower than 2, which is acceptable.

Table 2. Comparison of experiment and modeling of Ar metastable density for various discharge conditions

Gap	Conditions	Ar metastable density		Ref
		Experiment Ar^3P_2	Modeling $Ar^3P_2 = Ar^* \times 5/12$	
1mm	50 kHz 1000 V	Max 2.5×10^{10} cm^{-3}	Max 2.6×10^{10} cm^{-3}	[54]
2mm	50 kHz 0.28 Wcm^{-3}	Mean 6.5×10^{9} cm^{-3}	Mean 5×10^{9} cm^{-3}	[55]
2mm	5 MHz 350 V	Mean 4×10^{9} cm^{-3}	Mean 7×10^{9} cm^{-3}	[55]

4 Influence of the LF voltage amplitude on RF discharge

The aim of this work is to understand the influence of the LF voltage amplitude on the behavior of a dual frequency RF-LF DBD. For this purpose, the LF voltage amplitude applied at a constant power RF discharge is first varied over a range spanning from 0 to 1300 V, which is wide enough to determine the different discharge modes. Then, we focus on each mode to understand the discharge behavior.

4.1 Identification of the different modes

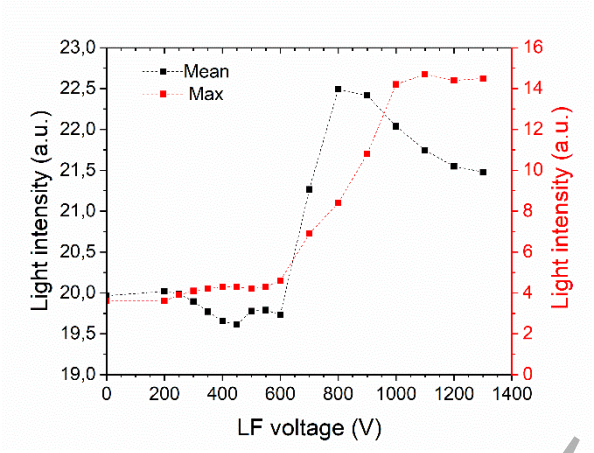

Figure 3. Mean and maximum of the light intensity of a DF-DBD for a RF voltage of 5 MHz and 350 V as a function of the 50 kHz voltage amplitude.

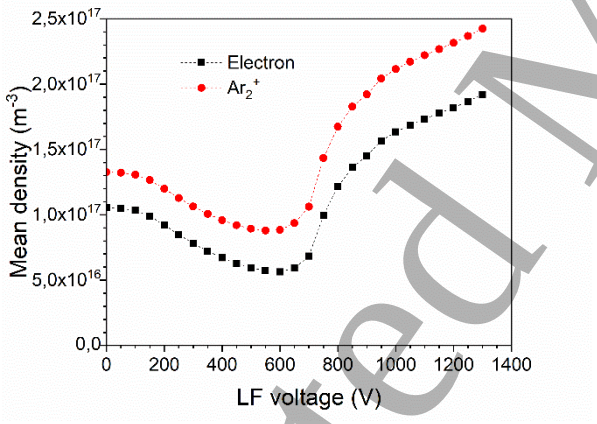

Figure 4. Mean density of electrons and ions calculated for a DF-DBD for a RF voltage of 5 MHz and 350 V as a function of the 50 kHz voltage amplitude.

A simple and efficient way to characterize a dual discharge consists of measuring the light intensity over both RF and LF time scale. The light intensity of DF-DBD observed for the same RF power is presented in Figure 3 as a function of the LF voltage. The variation of both the mean and the maximum intensity of the DF discharge with the LF voltage are rather similar. Both drastically increase from 600 V to 800 V for the mean intensity and to 1000 V for the maximum intensity. Below 600 V, the maximum light intensity is almost independent of the LF amplitude, then it increases by a factor of

3.5 between 600 and 1000 V before getting again independent of the LF voltage above 1000 V. This behavior allows to identify two modes: mode 1, below 600 V and mode 2, above 1000 V. For mode 1, the mean intensity decreases above 250 V, while for mode two that seems to be reached at 750 V, the intensity decreases beyond 900 V. The difference between the mean and the maximum of the light intensity is associated with the discharge dissymmetry at the RF scale. As an example, previous work has shown that the RF discharge could turn off during part of the RF cycle, which reduces the mean discharge power but not the maximum value [33].

Similar behavior is observed with the results of numerical modeling for the DF discharge in the same conditions as for experiments, i.e. a 5 MHz RF voltage amplitude of 350 V and a LF voltage amplitude ranging from 0 to 1300 V. As illustrated by the mean electron and ion densities shown in Figure 4, a steep variation is observed between 600 and 1000 V. The electron density is enhanced by a factor of 2 and that of ion by a factor of 3. Below 600 V, the densities decrease like the mean light intensity showing that the discharge weakens. Above 600 V, the density of electrons and ions increase.

Both experimental and numerical results indicate the presence of a transition in the discharge behavior at some LF voltage amplitude: mode 1 below 600 V and mode 2 above 600 V. In the following, our aim is to understand the differences between these modes. For this purpose, results obtained for discharge either in mode 1 or in mode 2 are discussed in detail. The voltages for each of these discharge are provided in Table 3. The RF-DBD corresponding to the same RF voltage (5 MHz, 350 V) is used as a reference. The low frequency is 50 kHz and the voltage amplitude is 400 V for the mode 1 and 1 kV for mode 2.

Table 3. Voltages used in the experimental and numerical studies for mode 1 and mode 2 DF-DBD

	RF	**V_{RF}**	**LF**	**V_{LF}**
RF-DBD	5 MHz	350 V	0	**0**
DF-DBD mode 1	5 MHz	350 V	50 kHz	**400 V**
DF-DBD mode 2	5 MHz	350 V	50 kHz	**1000 V**

4.2 Comparison of the different discharge modes

Before to consider space and time-resolved results, the relative contributions of the different reactions considered in the model (Table 4) are presented.

Table 4. Relative contributions of the most important reactions of Table 1 to the creation and loss of electrons, Ar^+ and Ar_2^+ ions and metastable atoms for the different discharge modes.

	RF	DF mode 1	DF mode 2
Electron			
Direct ionization (reaction 6)	0%	0.2%	15%
Penning ionization (9)	95%	95%	80%
Recombination of Ar_2^+ (2)	-7%	-5%	-10%
Ar^+ Ion	**RF**	**DF mode 1**	**DF mode 2**
Direct ionisation (6)	0%	0.2%	16%
Penning ionization (9)	99%	99%	83.50%
Stepwise ionisation (5)	0%	0%	0.2%
Ion conversion Ar^+ ->Ar_2^+ (10)	-100%	-100%	-100%
Ar_2^+ Ion	**RF**	**DF mode 1**	**DF mode 2**
Conversion Ar^+ -> Ar_2^+ (10)	100%	100%	99.80%
Metastable ionisation (5)	0%	0%	0.2%
Recombination of Ar_2^+ (2)	-7%	-5%	-10%
Metastables	**RF**	**DF mode 1**	**DF mode 2**
Direct excitation (1)	99%	99.5%	98.50%
Penning ionization (9)	-12%	-12%	-12%
Desexcitation (3)	-88%	-88%	-88%

Table 5. Mean and max of electron, ion and metastable atoms densities for the 3 discharge modes.

		RF	DF mode 1	DF mode 2
Electrons	Mean density	1.1×10^{17} m^{-3}	6.7×10^{16} m^{-3}	1.6×10^{17} m^{-3}
	Maximum value	1.5×10^{17} m^{-3}	1.3×10^{17} m^{-3}	6.3×10^{17} m^{-3}
Ar_2^+ ions	Mean density	1.3×10^{17} m^{-3}	9.6×10^{16} m^{-3}	2.1×10^{17} m^{-3}
	Maximum value	1.6×10^{17} m^{-3}	1.2×10^{17} m^{-3}	6.4×10^{17} m^{-3}
Metastable atoms	Mean density	4.3×10^{16} m^{-3}	3.1×10^{16} m^{-3}	1.3×10^{17} m^{-3}
	Maximum value	2.3×10^{17} m^{-3}	2.1×10^{17} m^{-3}	4.2×10^{18} m^{-3}

Among the 10 reactions considered in the collisional-radiative model, only seven play a significant role (Table 4). The electrons and Ar^+ ions are mostly created by Penning ionization (reaction 9) with a contribution of direct ionization (reaction 6) increasing from~0 for mode 1 to 15% for mode 2. This latter reaction involves electrons with more than 15.8 eV i.e. a large electric field. Ionization produces Ar^+ that is very efficiently converted in Ar_2^+ by the 3 body reaction 10. Subsequent ion loss due to dissociative recombination is small, only 5% for mode 1 and 10% for mode 2. However, it is important to note that a large part of these ions (99% for mode 1 and 83.5% for mode 2) are produced via reaction 9, which mimicks Penning ionization of NH_3, so that in reality they would not be argon ions at all but rather NH_3^+ ions. The ions loss due to dissociative recombination is rather low, 5 and 10% for mode 1 and mode 2 respectively. Both ions and electrons are mainly loss at the walls. Whatever the discharge regime is, the metastable atoms are mainly created from the ground-state level of Ar by electron collisions (reaction 1) while their losses are due to Penning ionization (12%) and to reaction 3 (88%). The mean and maximum densities of electrons, ions and metastable atoms is reported in Table 5 for the two DF modes and compared to those of the classical RF discharge. For a given mode, all species show a similar behavior. The difference between a RF and a DF mode 1 discharge is a decrease of all the species densities. The variation is less than a factor 2. From RF to DF mode 2 the densities increases. The maximum of the electron and ion density increase by a factor of 4 and the metastable

density by a factor of 18 while the mean density of the electron and ion slightly increase and the metastable density increases by a factor of 3.

To summarize, the contribution of the different reactions of Table 1 are similar for the RF and the DF mode 1 discharges, while for the DF mode 2 discharge, direct ionization is more important even if Penning ionization remains dominant. The ionization of the metastable states is always low. In DF mode 1, the discharge is weakened by the increase of the losses to the wall (or drift to the cathode), which lowers the densities of the species in contrast with DF mode 2 in which the discharge strengthens by the increase of these densities.

Spatially-resolved results across the gas gap, averaged over a LF cycle, are presented in Figure 5. For the three kinds of discharges, the mean density profiles of electrons, ions and metastable atoms as well as the electron temperature across the gap gas and the contribution of direct electron ionization are shown.

a)

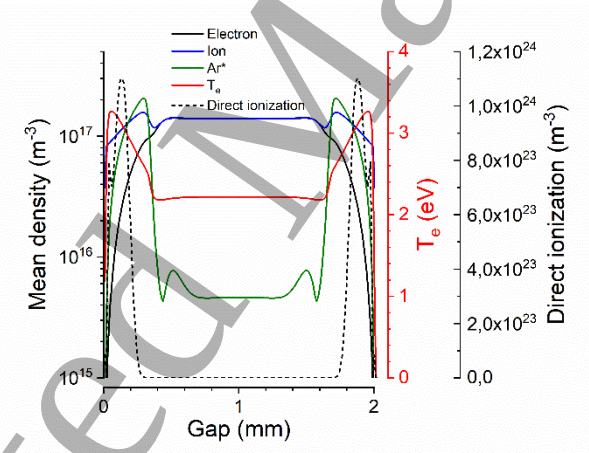

b) c)

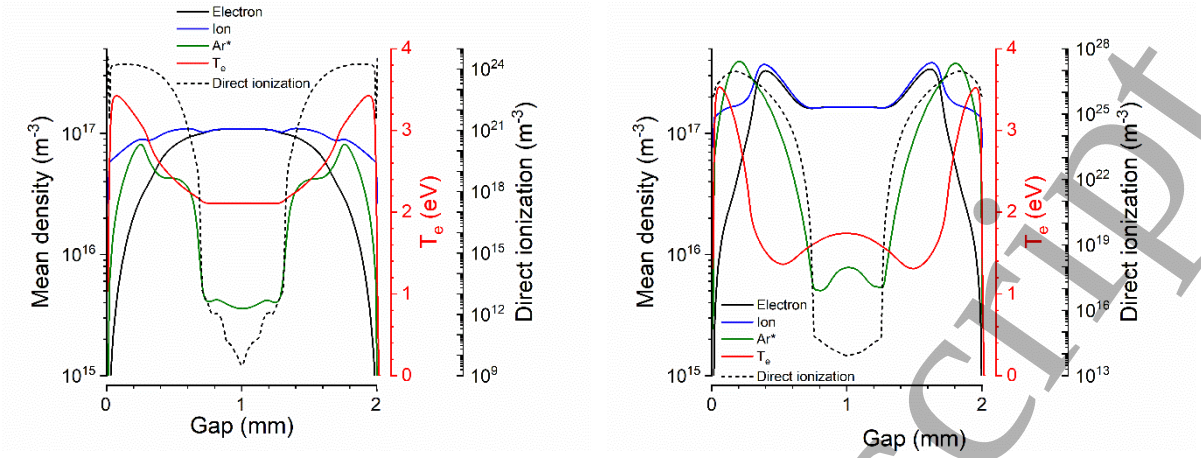

Figure 5. Electron temperature, direct ionization and mean density profiles of the electron, ion and metastable across the gap averaged on an LF cycle: (a) RF-DBD, (b) DF-DBD mode 1 and (c) DF-DBD mode 2.

The RF, DF mode 1 and 2 discharges are characterized by a cathode fall on each side of the plasma bulk showing that the density of ions is always large enough to make the RF electron oscillation induce a space-charge electric field. The three discharges are RF discharges. The maximum of the electron temperature is similar in these three cases (3.3 to 3.5 eV) and is located within the sheath, close to the cathode. Compared to the RF-DBD, in DF mode 1, the low LF voltage amplitude induces the cathode sheath expansion and decreases the plasma bulk and the density. This is explained by the increase of the ion loss due to the drift to the cathode by the LF electric field. It results in a decrease of the ion density and in a decrease of the electric field due to the electron RF oscillation. As compared to an RF discharge, the electron temperature remains high in a larger zone and the area where electrons, ions and metastable atoms are created is broader, their density decreases because of the enhanced loss to the cathode. The plasma bulk density is also reduced and the discharge weakens.

In DF mode 2 where the LF voltage amplitude is higher, all densities increase, the electron temperature (T_e) steeply decreases in the bulk. The T_e minimum value is at the sheath edge because of the high direct ionization in this area. The cathode fall thickness is similar to that in the RF discharge but with a stronger field and the formation of a negative glow. The higher LF voltage amplitude yields the increase of ionization over a wider zone and the plasma bulk further reduces as compared to the RF-

DBD. The maximum electron and ion density is observed where T_e reaches its minimum value that is half of that of the other modes, i.e. about 1 eV compared to 2 eV.

To summarize, applying a LF voltage reduces the average ion density in comparison with that of the RF discharge. This modifies the electric field distribution, but does not change the chemical kinetics. All species have their density reduced. At high LF voltage amplitude, the ion density increases and the cathode fall length shrinks while direct ionization mainly occurs at the edge of the cathode fall. The next step is to determine when the variation of the densities species and the electric field occur. This is the aim of the following paragraph where experimental (Figure 6) and numerical results are presented with space and time resolution (Figure 7).

Figure 6 shows the space and time variation of the light intensity over a LF half cycle. Pictures are taken with an ICCD camera using an exposure time equal to the RF period (200 ns). For each picture, light is integrated over the 8 mm plasma length leading to light distribution over the gas gap. Phase resolved [30] emission, i.e. emission profiles from one electrode to the other over a half LF cycle are presented for the 3 discharges modes in Figure 6. As the configuration is fully symmetric, for the sake of clarity, results are presented on a half cycle i.e. 10 µs. Time 0 corresponds to the maximum of the LF applied voltage and 10 µs to its minimum. The main emission detected by the iCCD camera is a continuum related to the high electronic density of the RF discharge [14][56]. The figure also presents the oscillogram of the voltage applied onto the electrodes and the measured current.

a) b) c)

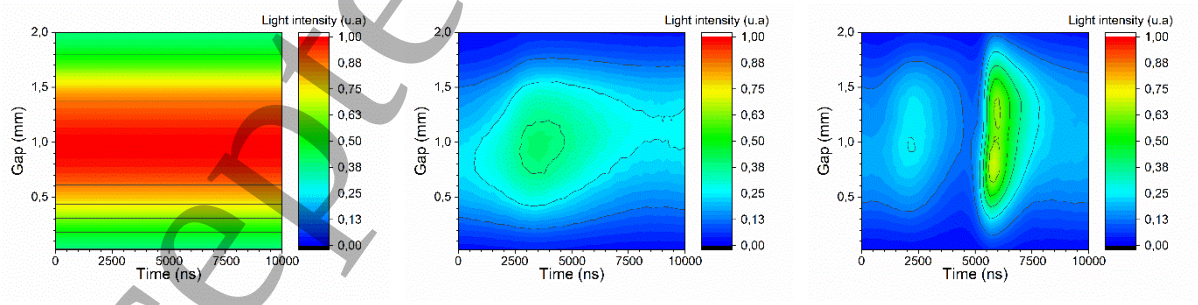

d) e) f)

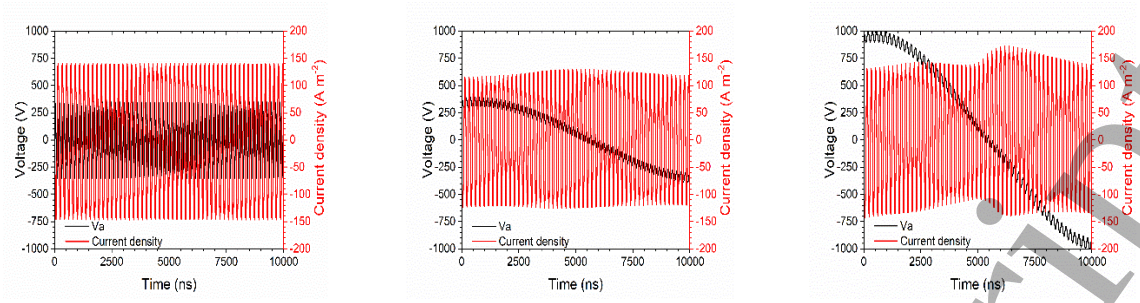

Figure 6. Phase-resolved discharge emission over one half LF cycle for: (a) the RF-DBD, (b) the DF-DBD mode 1 and (c) the DF-DBD mode 2. Voltage applied onto the electrode V_a, and the measured current density over one half LF cycle for: (d) the RF-DBD, (e) the DF-DBD mode 1 and (f) the DF-DBD mode 2.

Figures 6a and 6d show the space-resolved light intensity (Fig. 6a) as well as the voltage and current density (Fig. 6d) as a function of time for the RF discharge. Clearly both emission and current density are uniform at the LF scale. The maximum emission occurs in the plasma bulk. This emission is mainly due to the continuum which is related to the electron density. Thus, an emission localized in the gas bulk could be related to a high electron density. This feature is characteristic of an α-RF discharge at atmospheric pressure [14]. For a DF discharge in mode 1 (Figure 6b), the maximum emission always takes place in the bulk showing that the discharge mode is the same as that of the RF and is an α-RF. However, the LF modulates this α-RF discharge. Both light emission and current are time modulated with an increase from 2.5 to 5 µs i.e. in the region where the LF voltage amplitude is weak. The maximum of the light emission and the current occur before V_a = 0 V, but due to the capacitive configuration of the DBD reactor, the voltage applied to the gas, V_g, is equal to 0 before V_a [47]. Ion drift is proportional to V_g and not to V_a and these observations show that lower is the LF voltage amplitude applied to the gas, higher is the discharge power and the ionization. In other words, lower is the ion extraction from the gas bulk higher is the discharge power. The ion loss is the reason why light intensity at low LF voltage amplitude in DF mode 1 is always lower than the RF discharge.

For a LF voltage amplitude of 1000 V, when the discharge is in DF mode 2 (Figure 6c), the light intensity gets larger than for the RF discharge. The discharge behavior depends on the LF voltage

polarity. When LF voltage is positive, from 1 to 5 µs, the light intensity is larger in the middle of the gap with a modulation similar to that of the DF mode 1, reaching a maximum around 2.5 µs which is expected to correspond to $V_g = 0$ V. When LF voltage is negative, from 5 and 10 µs, the variation of the light intensity over the half cycle is larger. The maximum of the emission is significantly stronger and the maximum are not in the middle of the gap but shifted closer to the electrodes. These maxima last for about 1.5 µs and they are correlated with a current maximum increase. In an atmospheric pressure RF discharge, the localization of the light close to the electrode is attributed to a γ mode [17]. In a γ-RF discharge, a large part of the seed electrons are cathode secondary electrons. As they are accelerated by the cathode fall, they have enough energy to make direct ionization which is in agreement with the increase of the direct ionization (Table 4) and the field and charge distribution shown in Figure 5c.

The model enables the understanding of the observations just reported. The gas voltage, the electric field and the electron and metastable densities across the gap are shown in Figure 7 for the RF discharge and the two DF discharge modes. The results are presented on a half cycle i.e. 10 µs as it was the case for the experimental results. Time 0 ns corresponds to the maximum LF applied voltage and 10 µs to its minimum.

RF-DBD DF-DBD ***(mode 1)*** DF-DBD ***(mode 2)***

a) b) c)

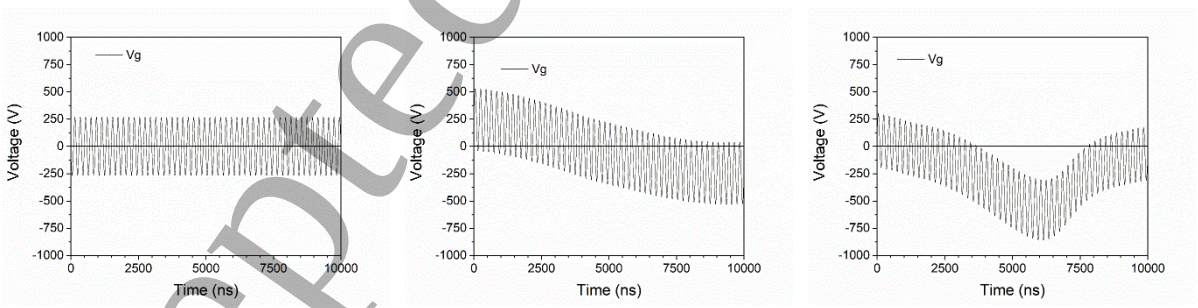

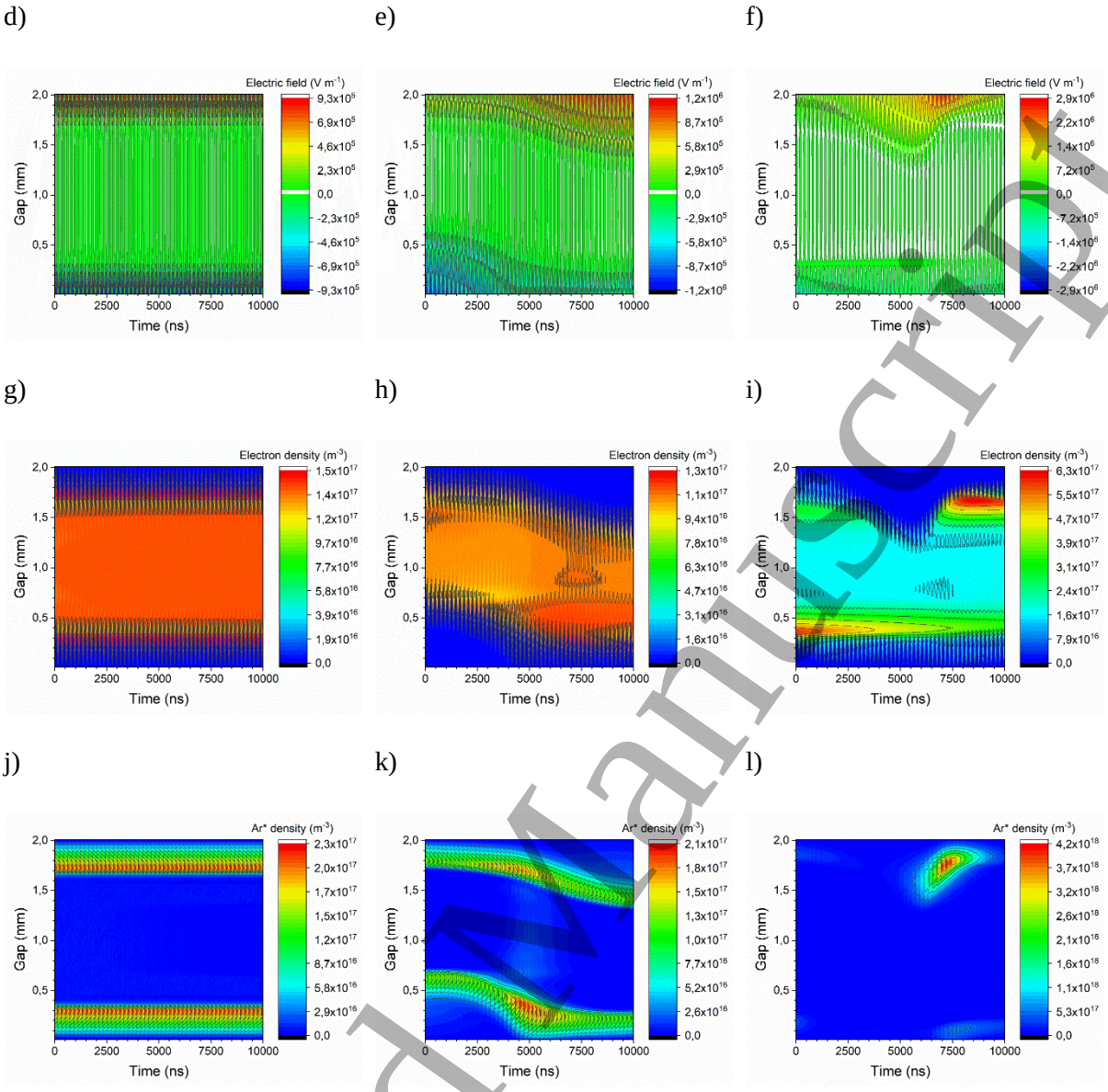

Figure 7. Simulated Space and time variation of the gas voltage (a-c) and spatio-temporal profiles of the electric field (d-f), the electron density (g-i) and the metastable density (j-l) for the different discharges mode across the gap and over half a cycle of the LF voltage.

As shown in Figure 7j, in absence of LF voltage, the metastable density is maximum at about 300 µm from the cathode, at the sheath edge. The electron density maximum occurs within the plasma bulk, where the electric field is weak. Due to the RF voltage, the electrons oscillate over a distance 500 µm from the dielectric surface. As the LF voltage amplitude increases, the gas voltage is modified as well as the electric field, hence the electron and metastable densities. In the DF-DBD mode 1, these parameters behave similarly to those of the RF-DBD. In agreement with the experiments, the electron

density remains maximum within the bulk (Figure 7h), which shows that the discharge still behaves like an α-RF discharge. A consequence of the LF voltage is that half of the time ionization takes place farther from the cathode because of the modulation of the sheath thickness by the LF component. The sheath length expands from about 500 µm to 900 µm on the side of the electrode biased with a negative LF voltage. This expansion of the sheath is explained by a lower ion density due to the higher ion loss at the cathode. Due to the RF voltage, the electron depleted zone always oscillate at the RF scale with an amplitude of 500 µm. For a high LF voltage amplitude, i.e. in the DF mode 2, ionization is clearly higher than in the case of the RF discharge. In comparison with the RF-DBD, the electric field maximum as well as the electron and metastable densities are enhanced by factors of 3, 4 and 20, respectively. The electric field maximum is achieved when V_g is maximum while the peak of the densities occurs later and is located at the sheath edge. The electric field and the densities are high only over a short period of time around 3 µs as compared to the 10 µs of the half cycle. This behavior is in very good agreement with the phase-resolved emission spectroscopy and it is similar to the characteristics of a typical DBD with a current pulse associated to a gas voltage drop stopping the ionization. This is confirmed by comparing the results with the space and time-resolved electrical field and electron and metastable densities of a 50 kHz, 1 kV, LF discharge. The maximum and the depletion zone are very similar showing that there is a common ionization mechanism. In the glow DBD, ion bombardment at the cathode is the main source of secondary electrons. One can therefore conclude that the high amplitude of the LF voltage is associated with a large secondary electron emission from the cathode, when the LF and RF polarities are the same. When they are out of phase, LF makes the ions drift toward the RF anode but the secondary electrons cannot ionize the gas due to the RF voltage. This is illustrated in Figure 9 that presents the metastable density over 3 RF cycles when V_g is maximum. Clearly, the metastable density only increases during half of the RF cycle. Comparing Figure 8b (LF discharge) and Figure 7i (mode 2 of DF discharge) clearly shows that RF always plays a dominant role, allowing a large increase of the electron density in the gas bulk from 10^{10} to several $10^{11}/cm^3$. This comparison also illustrates why the γ-RF mode generated by the dual frequency is diffuse: the density of electrons remains always large, a condition favoring the achievement of a diffuse discharge.

a) b)

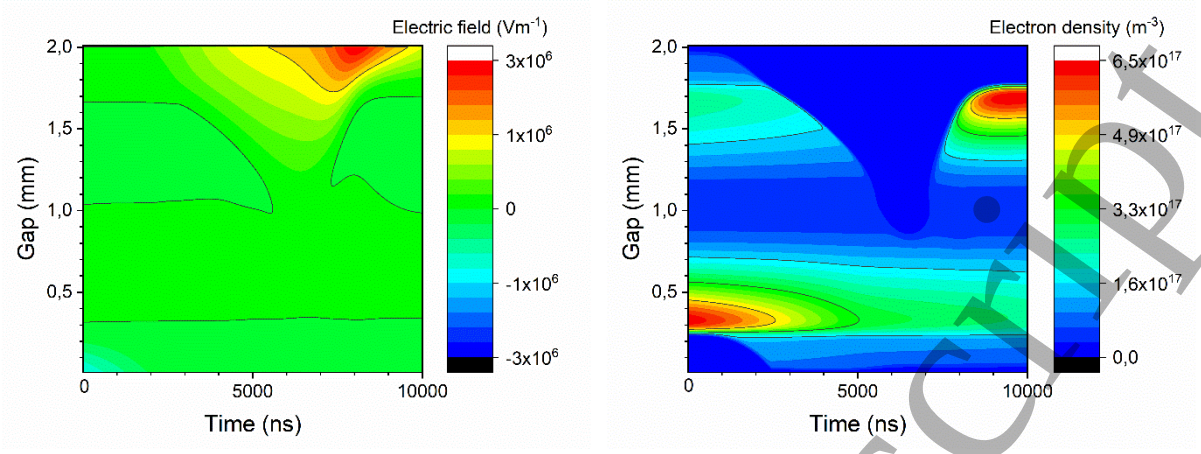

c)

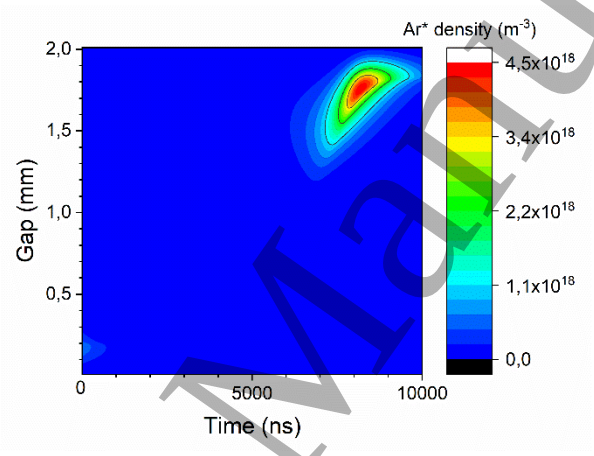

Figure 8. Space and time distribution of the (a) electric field, (b) electron density and (c) metastable density of a LF-DBD (50 kHz, 1000 V).

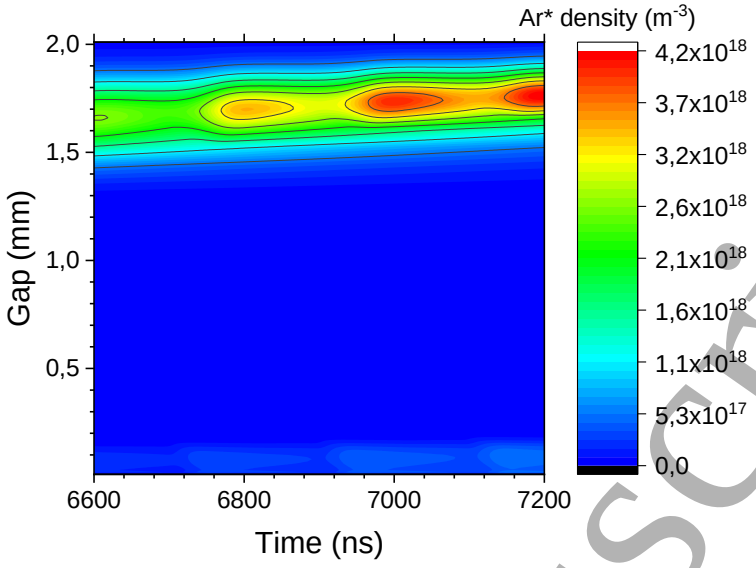

Figure 9. Space and time distribution of the metastable density in DF mode 2 discharges during 3 RF cycles at the maximum of the LF voltage amplitude.

The variation of electron production over a LF half cycle also well illustrates the influence of the LF voltage. As shown in Figure 10, the electron production integrated over the gap is strongly modified by the LF components.

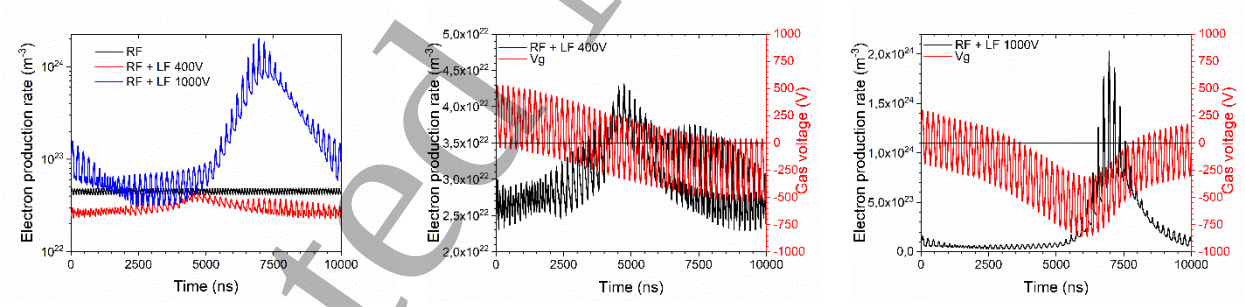

Figure 10. Time evolution of the electron production rate over half a LF cycle (a) for the RF-DBD, the DF-DBD in mode 1 and the DF-DBD in mode 2. Comparisons of gas voltage and electron production for (b) DF mode 1 and (c) DF mode 2.

Figure 10a compares the electron production of the RF discharge and the two discharge modes of DF-DBD. Production is reduced by applying low amplitude LF and it is enhanced by high amplitude

LF over part of the half cycle. The electron production rate oscillates at twice the RF frequency. In Figure 10 b and c, these variations are compared to the gas voltage.

For DF mode 1, the maximum electron production is observed when the LF voltage applied (V_{LF}) is zero, as for the metastable atom density shown in Figure 7k. This supports the previous explanation provided, i.e. when $V_{LF} = 0$ V, the ions are no more extracted from the sheath, their density is higher, the cathode sheath is thinner, and the electric field and the electron temperature reach higher values, which results in a larger ionization rate. The electron production rate value reaches 4.4×10^{22} m^{-3}, which is slightly lower than for the RF-DBD even when $V_{LF} = 0$ V, because ions lifetime is larger than the RF cycle. The production rate decreases to 2.3×10^{22} m^{-3} when the LF voltage reaches its maximum because the extraction at the cathode is maximum.

In DF mode 2, the ionization rate is low during the first part of the cycle. It is similar to that observed for the RF discharge and the DF-DBD discharge in mode 1. From a gas voltage of about 500 V, the ionization rate increases and V_g is maximum right after that. This is the behavior of a low frequency DBD: when the ionization increases, the solid dielectrics are charged and the gas voltage decreases. The γ-mode occurs about 1/5 of the LF cycle. The maximum of the metastable atom density (Figure 7l) is reached when the production of electron is maximum (Figure 10c).

For each RF cycle, the oscillation of discharge characteristics at the RF scale is due to the alternation between additive and subtractive amplitude of the LF and RF components. The oscillation amplitude of the ionization rate at the RF scale is minimum when the LF voltage is zero, as clearly observed in Figure 10c. For DF mode 2, the ionization rate reaches its minimum right after V_{LF} minimum and is equal to that of DF mode 1.

Both DF modes 1 and 2 show a peak of electron production, but their origin are quite different. For DF mode 1, the peak is observed when the V_{LF} is zero because of ion extraction from the gas is reduced. For DF mode 2, the peak starts when V_g is maximum and its amplitude is 50 times higher, indicating a new ionization mechanism occurs. A larger contribution of direct ionization from 0 to 15% takes place together with a larger ion drift to the cathode, hence a higher secondary emission when the polarities of RF and LF are identical.

For the two DF-DBD modes, the sheath can be seen as the superposition of RF and LF sheaths. The "LF sheath" is defined by the ion density: higher is this density shorter the sheath is. The "RF sheath" thickness oscillates with the RF voltage. This oscillation amplitude stays the same but its spatial position is defined by the "LF sheath".

The drastic modifications observed in the DF mode 2 of the DF-DBD are attributed to the additional ionization due to the LF component. It is controlled by the gas voltage which like in a low frequency DBD depends on the charge of the dielectrics. The ion flux to the wall and the emission of the secondary electron as a function of the time are presented in Figure 11. The electron flux is negative as it corresponds to the secondary emission.

a) b) c)

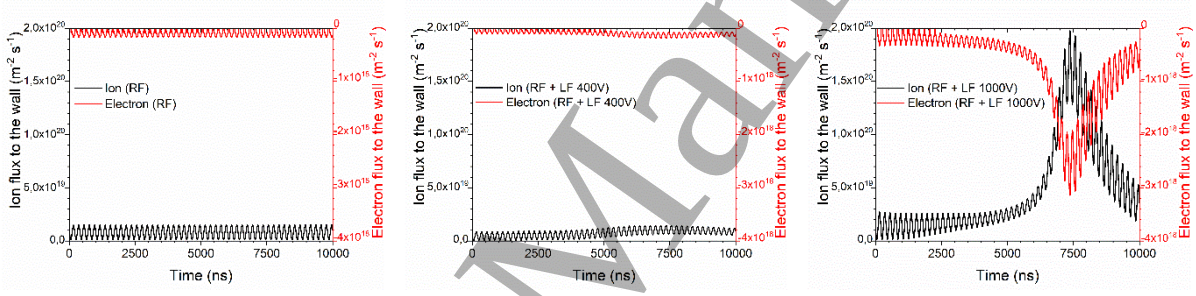

Figure 11. Ion flux to the wall and secondary electron emission flux for: (a) RF-DBD, (b) DF-DBD in mode 1 and (c) DF-DBD in mode 2

Both the ion flux to the wall and the secondary electron flux increase with the LF voltage amplitude and their maximum take place simultaneously. Secondary emission could also be due to metastable. However, the flux of metastable atoms is negligible as compared to that of ions.

5 Conclusion

The effect of the LF voltage amplitude on an α-RF-DBD of constant power is studied through 1D-simulation and experiments. Both numerical and experimental results point out two distinct discharge modes which depends on the V_{LF} amplitude. For a 2 mm gap and a 350 V, 5 MHz RF discharge, the transition is observed for LF voltage amplitude between 600 V and 1000 V. For V_{LF}

lower than 600 V, the DF is an α-RF, for higher V_{LF}, around the maximum of the gas voltage, the α-RF discharge becomes a γ-RF for about 3 µs each half cycle of V_{LF}.

Whatever its value, V_{LF} drifts ions to the LF cathode and secondary electrons are produced when the RF and LF cathode are the same electrode. These electrons are multiplied in the gas bulk according to an amplification rate that depends on the voltage applied to the gas. This voltage is equal to the sum of LF and RF voltage minus the voltage applied to the dielectric, V_{ds}. In a RF discharge, V_{ds} is negligible, in a DF discharge it increases with the drift of the bulk charge to the electrodes i.e. V_{LF} amplitude. On one hand, V_{LF} induces a loss of ions at the LF cathode, on the other hand, these ions produce secondary electrons which are multiplied by the RF discharge. The discharge regime depends on the equilibrium between the loss and the creation of the ions.

For low V_{LF}, the secondary ionization is low and the discharge physics is controlled by the ion loss. The gas bulk ion density and thus electron density decrease when V_{LF} increases. The RF plasma density is lower than that of the RF discharge. The flux of ion at the cathode depends on the instantaneous V_{LF} amplitude, higher it is, higher is the loss and larger is the cathode sheath. Consequently, during a LF cycle the plasma density oscillates. It is maximum when $V_{LF} = 0$ V and minimum when V_{LF} is maximum. For an LF voltage amplitude equal to 1000 V, the voltage applied to the gas reach values high enough to enhance the secondary ionization to such a point that the physics of the discharge depends on the secondary electrons multiplication at the sheath edge. The γ mode is observed. γ and α mode alternate at the RF frequency and the discharge is a dielectric barrier controlled discharge. The stability of this γ mode is explained by the rather low increase of the electron density compared to the α-mode and by the fact that the duration of the γ-mode is only 1/5 of LF cycle (figure 10c) which limits overheating.

The DF discharge with a high LF voltage amplitude is promising for PECVD because of the high densities of electrons and metastables which should ensure an efficient dissociation of the thin film precursors with a homogeneous discharge and because of the ion flux to the surface which should be efficient to densify the coating. In order to complete this study, the next work in progress is focusing on the transition between these modes, the importance of the secondary electron emission coefficient and the influence of the RF voltage amplitude.

References

[1] F. Massines and G. Gouda, "A comparison of polypropylene-surface treatment by filamentary, homogeneous and glow discharges in helium at atmospheric pressure," *J. Phys. D. Appl. Phys.*, vol. 31, no. 24, pp. 3411–3420, 1998.

[2] U. Kogelschatz, "Dielectric Barrier Discharge : Their History, Discharge Physic, and Industrial Applications," *Plasma Chem. Plasma Process.*, vol. 23, no. 1, pp. 1–46, 2003.

[3] B. Dong, J. Bauchire, J. Pouvesle, P. Magnier, and D. Hong, "Experimental study of a DBD surface discharge for the active control of subsonic airflow," *J. Phys. D. Appl. Phys.*, vol. 41, 2008.

[4] M. Gelker, C. C. Müller-Goymann, and W. Viöl, "Permeabilization of human stratum corneum and full-thickness skin samples by a direct dielectric barrier discharge," *Clin. Plasma Med.*, vol. 9, pp. 34–40, 2018.

[5] P. Brunet, R. Rincón, Z. Matouk, M. Chaker, and F. Massines, "Tailored Waveform of Dielectric Barrier Discharge to Control Composite Thin Film Morphology," *Langmuir*, vol. 34, no. 5, pp. 1865–1872, 2018.

[6] Q. H. Trinh, M. M. Hossain, S. H. Kim, and Y. S. Mok, "Tailoring the wettability of glass using a double-dielectric barrier discharge reactor," *Heliyon*, vol. 4, no. 1, p. e00522, 2018.

[7] B. Ghimire, D. P. Subedi, and R. Khanal, "Improvement of wettability and absorbancy of textile using atmospheric pressure dielectric barrier discharge," *Cit. AIP Adv.*, vol. 7, no. 085213, 2017.

[8] O. Levasseur, M. Vlad, J. Profili, N. Gherardi, A. Sarkissian, and L. Stafford, "Deposition of fluorocarbon groups on wood surfaces using the jet of an atmospheric-pressure dielectric barrier discharge," *Wood Sci. Technol.*, vol. 51, no. 6, pp. 1339–1352, 2017.

[9] J. Profili, O. Levasseur, J. B. Blaisot, A. Koronai, L. Stafford, and N. Gherardi,

"Nebulization of Nanocolloidal Suspensions for the Growth of Nanocomposite Coatings in Dielectric Barrier Discharges," *Plasma Process. Polym.*, vol. 13, no. 10, pp. 981–989, 2016.

[10] R. Bazinette, J. F. Lelièvre, L. Gaudy, and F. Massines, "Influence of the Discharge Mode on the Optical and Passivation Properties of SiNx:H Deposited by PECVD at Atmospheric Pressure," *Energy Procedia*, vol. 92, pp. 309–316, 2016.

[11] J. Vallade *et al.*, "A-SiNx:H antireflective and passivation layer deposited by atmospheric pressure plasma," *Energy Procedia*, vol. 27, pp. 365–371, 2012.

[12] R. Bazinette, J. Paillol, J. F. Lelièvre, and F. Massines, "Atmospheric Pressure Radio-Frequency DBD Deposition of Dense Silicon Dioxide Thin Film," *Plasma Process. Polym.*, vol. 13, no. 10, pp. 1015–1024, 2016.

[13] F. Massines *et al.*, "Hydrogenated Silicon Nitride SiNx:H Deposited by Dielectric Barrier Discharge for Photovoltaics," *Plasma Process. Polym.*, vol. 13, no. 1, pp. 170–183, 2016.

[14] R. Bazinette, J. Paillol, and F. Massines, "Optical emission spectroscopy of glow, Townsend-like and radiofrequency DBDs in an Ar/NH3mixture," *Plasma Sources Sci. Technol.*, vol. 24, no. 5, 2015.

[15] R. Bazinette, R. Subileau, J. Paillol, and F. Massines, "Identification of the different diffuse dielectric barrier discharges obtained between 50kHz to 9MHz in Ar/NH3 at atmospheric pressure," *Plasma Sources Sci. Technol.*, vol. 23, no. 3, 2014.

[16] J. J. Shi, D. W. Liu, and M. G. Kong, "Plasma stability control using dielectric barriers in radio-frequency atmospheric pressure glow discharges," *Appl. Phys. Lett.*, vol. 89, no. 8, pp. 8–10, 2006.

[17] J. J. Shi and M. G. Kong, "Mode transition in radio-frequency atmospheric argon discharges with and without dielectric barriers," *Appl. Phys. Lett.*, vol. 90, no. 10, 2007.

[18] J. Schulze, E. Schüngel, U. Czarnetzki, and Z. Donkó, "Optimization of the electrical asymmetry effect in dual-frequency capacitively coupled radio frequency discharges: Experiment, simulation, and model," *J. Appl. Phys.*, vol. 106, no. 6, 2009.

[19] J. Schulze, Z. Donkó, D. Luggenhölscher, and U. Czarnetzki, "Different modes of electron heating in dual-frequency capacitively coupled radio frequency discharges," *Plasma Sources Sci. Technol.*, vol. 18, no. 3, 2009.

[20] Z. Donkó, J. Schulze, B. G. Heil, and U. Czarnetzki, "PIC simulations of the separate control of ion flux and energy in CCRF discharges via the electrical asymmetry effect," *J. Phys. D. Appl. Phys.*, vol. 42, no. 2, 2009.

[21] T. Kitajima, Y. Takeo, Z. L. Petrović, and T. Makabe, "Functional separation of biasing and sustaining voltages in two-frequency capacitively coupled plasma Functional separation of biasing and sustaining voltages in two-frequency capacitively coupled plasma," *Appl. Phys. Lett.*, vol. 489, no. 2000, pp. 1–4, 2006.

[22] Z. L. Zhang, J. W. M. Lim, Q. Y. Nie, X. N. Zhang, and B. H. Jiang, "Electron heating and mode transition in dual frequency atmospheric pressure argon dielectric barrier discharge Electron heating and mode transition in dual frequency atmospheric pressure argon dielectric barrier discharge," *AIP Adv.*, vol. 7, no. 10, p. 105313, 2017.

[23] C. Oneill, J. Waskoenig, and T. Gans, "Tailoring electron energy distribution functions through energy confinement in dual radio-frequency driven atmospheric pressure plasmas," *Appl. Phys. Lett.*, vol. 101, no. 15, pp. 1–5, 2012.

[24] T. Gans, D. O'Connell, V. Schulz-Von Der Gathen, and J. Waskoenig, "The challenge of revealing and tailoring the dynamics of radio-frequency plasmas," *Plasma Sources Sci. Technol.*, vol. 19, no. 3, 2010.

[25] J. Waskoenig and T. Gans, "Nonlinear frequency coupling in dual radio-frequency driven atmospheric pressure plasmas," *Appl. Phys. Lett.*, vol. 96, no. 18, 2010.

[26] Y. J. Zhou, Q. H. Yuan, F. Li, X. M. Wang, G. Q. Yin, and C. Z. Dong, "Nonequilibrium atmospheric pressure plasma jet using a combination of 50 kHz/2 MHz dual-frequency power sources," *Phys. Plasmas*, vol. 20, no. 11, 2013.

[27] F. R. Kong, Z. L. Zhang, and B. H. Jiang, "Numerical study of the discharge properties of atmospheric dielectric barrier discharge by using 200 kHz/13.56 MHz excitations," *AIP Adv.*, vol. 8, no. 7, 2018.

[28] F. Massines, R. Bazinette, and J. Paillol, "RF-LF dual frequency uniform dielectric barrier discharge for thin film processing," *22nd Int. Symp. Plasma Chem.*, pp. 1–5, 2015.

[29] Y. Liu, S. A. Starostin, F. J. J. Peeters, M. C. M. Van De Sanden, and H. W. De Vries, "Atmospheric-pressure diffuse dielectric barrier discharges in Ar/O2gas mixture using 200 kHz/13.56 MHz dual frequency excitation," *J. Phys. D. Appl. Phys.*, vol. 51, no. 11, 2018.

[30] Y. Liu, F. J. J. Peeters, S. A. Starostin, M. C. M. Van De Sanden, and H. W. De Vries, "Improving uniformity of atmospheric- pressure dielectric barrier discharges using dual frequency excitation," *Plasma Sources Sci. Technol.*, 2018.

[31] P. J. Bruggeman, F. Iza, and R. Brandenburg, "Foundations of atmospheric pressure non-equilibrium plasmas," *Plasma Sources Sci. Technol*, vol. 26, 2017.

[32] A. Berchtikou, J. Lavoie, V. Poenariu, B. Saoudi, R. Kashyap, and M. Wertheimer, "Thermometry in noble gas dielectric barrier discharges at atmospheric pressure using optical emission spectroscopy," *IEEE Trans. Dielectr. Electr. Insul.*, vol. 18, pp. 24–33, 2011.

[33] R. Bazinette, "in preparation," *Plasma Sources Sci. Technol.*, 2019.

[34] G. J. M. Hagelaar, G. Fubiani, and J.-P. Boeuf, "Model of an inductively coupled negative ion source : I . General model description," *Plasma Sources Sci. Technol.*, vol.

20, 2011.

[35] J. Gregorio, X. Aubert, G. J. M. Hagelaar, V. Puech, and L. C. Pitchford, "Nanosecond-pulsed dielectric barrier discharges in Kr / Cl 2 for production of ultraviolet radiation," *Plasma Sources Sci. Technol.*, vol. 23, 2014.

[36] G. J. M. Hagelaar and L. C. Pitchford, "Solving the Boltzmann equation to obtain electron transport coefficients and rate coefficients for fluid models," *Plasma Sources Sci. Technol.*, vol. 14, 2005.

[37] "BOLSIG+ software, https://www.bolsig.laplace.univ-tlse.fr,version 03/2016." .

[38] "Yamabe, Buckman, and Phelps, Phys. Rev. 27,1345 (1983). Revised Oct 1997."

[39] "PHELPS database, https://www.lxcat.laplace.univ-tlse.fr, retrieved June 4, 2013." .

[40] F. J. Mehr and M. A. Biondi, "Electron-temperature dependence of electron-ion recombination in Argon," *Phys. Rev.*, vol. 176, no. 1, pp. 322–326, 1968.

[41] C. M. Ferreira, J. Loureiro, and A. Ricard, "Populations in the metastable and the resonance levels of argon and stepwise ionization effects in a low-pressure argon positive column," *J. Appl. Phys.*, vol. 57, no. 1, pp. 82–90, 1985.

[42] R. A. Arakoni, A. N. Bhoj, and M. J. Kushner, "H2 generation in Ar/NH3 microdischarges," *J. Phys. D. Appl. Phys.*, vol. 40, no. 8, pp. 2476–2490, 2007.

[43] S. K. Lam, C.-E. Zheng, D. Lo, A. Dem'yanov, and A. P. Napartovich, "Kinetics of Ar * 2 in high-pressure pure argon," *J. Phys. D. Appl. Phys.*, vol. 33, no. 3, pp. 242–251, 2000.

[44] N. Balcon, G. J. M. Hagelaar, and J. P. Boeuf, "Numerical model of an argon atmospheric pressure RF discharge," *IEEE Trans. Plasma Sci.*, vol. 36, no. 5 SUPPL. 4, pp. 2782–2787, 2008.

[45] S. Y. Moon, W. Choe, and B. K. Kang, "A uniform glow discharge plasma source at atmospheric pressure," *Appl. Phys. Lett.*, vol. 84, no. 2, pp. 188–190, 2004.

[46] M. Moravej, X. Yang, G. R. Nowling, J. P. Chang, R. F. Hicks, and S. E. Babayan, "Physics of high-pressure helium and argon radio-frequency plasmas," *J. Appl. Phys.*, vol. 96, no. 12, pp. 7011–7017, 2004.

[47] F. Massines, N. Gherardi, N. Naudé, and P. Ségur, "Glow and Townsend dielectric barrier discharge in various atmosphere," *Plasma Phys. Control. Fusion*, vol. 47, no. 12 B, pp. 577–588, 2005.

[48] F. Massines, A. Rabehi, P. Decomps, R. Ben Gadri, P. Ségur, and C. Mayoux, "Experimental and theoretical study of a glow discharge at atmospheric pressure controlled by dielectric barrier," *J. Appl. Phys.*, vol. 83, no. 6, pp. 2950–2957, 1998.

[49] and F. M. I. Enache, N. Naude, J.P. Cambronne, N. Gherardi, "Electrical model of the atmospheric pressure glow discharge (APGD) in helium," *Eur. Phys. J. Appl. Phys.*, pp. 15–21, 2005.

[50] Y. B. Golubovskii, V. A. Maiorov, J. Behnke, and J. F. Behnke, "Modelling of the homogeneous barrier discharge in helium at atmospheric pressure," *J. Phys. D. Appl. Phys.*, vol. 36, no. 1, pp. 39–49, 2003.

[51] E. Carbone, E. Van Veldhuizen, G. Kroesen, and N. Sadeghi, "Electron impact transfer rates between metastable and resonant states of argon investigated by laser pump – probe technique," *J. Phys. D. Appl. Phys.*, vol. 48, 2015.

[52] E. Carbone *et al.*, "Spatio-temporal dynamics of a pulsed microwave argon plasma : ignition and," *Plasma Sources Sci. Technol.*, vol. 24, 2015.

[53] E. A. D. Carbone, S. Hubner, J. J. A. M. van der Mullen, G. M. W. Kroesen, and N. Sadeghi, "Determination of electron-impact transfer rate coefficients between argon 1s 2 and 1s 3 states by laser pump – probe technique," *J. Phys. D. Appl. Phys.*, vol. 46, 2013.

[54] S. Pouliquen, "Etude d'une nouvelle décharge à barrière diélectrique homogène en

mélange Ar/NH3/SiH4 à la pression atmosphérique pour le dépôt en continu de SiNx:H sur cellule photovoltaïque silicium," PhD, Université de Perpignan, 2010.

[55] R. Bazinette, "Effet de la forme d'excitation électrique sur une décharge par barrière diélectrique (DBD) à la pression atmosphérique et application au dépôt de couche mince," PhD, Université de Perpignan, 2016.

[56] P. Ranson *et al.*, "Étude expérimentale de l ' émission de Bremsstrahlung électron atome dans un jet de plasma d ' argon," *Rev. Phys. Appl.*, vol. 12, pp. 1829–1834, 1977.